JOURNAL OF Materials CHEMISTRY

Synthesis of high surface area monoclinic WO_3 particles using organic ligands and emulsion based methods

Zhixiang Lu,[a,b] Sofian M. Kanan[a] and Carl P. Tripp*[a,b]

[a]*Laboratory for Surface Science and Technology (LASST), University of Maine, Orono, ME 04469, USA. Tel: 207-5812235; Fax: 207-5812255; E-mail: ctripp@maine.edu*
[b]*Department of Chemistry, University of Maine, Orono, ME 04469, USA*

Received 30th August 2001, Accepted 13th January 2002
First published as an Advance Article on the web 25th February 2002

Several synthetic approaches have been used to obtain nano-sized monoclinic WO_3 (m-WO_3) powders. All of these methods begin with a standard preparative method where H_2WO_4 is first generated by passing a Na_2WO_4 solution through a cation-exchange resin. It is shown that high surface area particles are produced by dripping the H_2WO_4 exiting from the ion-exchange column into a solution containing oxalate and acetate exchange ligands or alternatively, into a water-in-oil (w/o) based emulsion. In comparison to commercial WO_3 powders, the surface area of the m-WO_3 powders were higher by factors of 10 and 20 times when prepared in the presence of acetate/oxalate chelating agents and w/o emulsions, respectively. The much higher surface areas enable infrared spectroscopic identification of surface sites along with detection and monitoring of gaseous reactions and adsorbed species on the surface of this metal oxide. This is demonstrated with the adsorption of a nerve agent simulant, dimethyl methyl phosphonate. In general, little is known about the reactions of gaseous molecules on m-WO_3 surfaces and the fabrication of high surface area m-WO_3 particles will aid in gaining an understanding of the chemical processes occurring in WO_3 based sensors.

Introduction

The development of sensors based on semiconductive monoclinic tungsten oxide (m-WO_3) has generated considerable interest because of their high sensitivity for the detection of gaseous adsorbates and because they are amenable to microfabrication techniques.[1–4] Typically, the active sensor element consists of an ultrahigh vacuum (UHV) controlled fabrication of a thin film of m-WO_3 mounted on a sapphire substrate containing the necessary electrodes, heating element and associated electronics. Alternatively, nano-sized metal oxide particles can be used to fabricate thick film sensors using a screen-printing process.[5–9] In both cases, the sensor generates a signal when the adsorption of gaseous molecules on the m-WO_3 sensor surface leads to a detectable change in conductivity of the oxide. However, as was found for all metal oxide based sensors, the lack of detection selectivity and sensor-to-sensor reproducibility continues to interfere with the fabrication of reliable devices for field operation.

Little is known about the source of poor selectivity and reproducibility. This is due in part to a lack of knowledge of the surface sites on WO_3 and surface reactions and species that occur on the WO_3 surface are exposed to various gases. In contrast, there is abundant literature on surface reactions occurring on other metal oxide surfaces.[10–18] A primary source of this data has been derived for infrared spectroscopic studies on nano-sized powders. The high surface area of the nanoparticulates enables spectroscopic detection of bands due to surface bonds and adsorbed species on the surface. Similar studies on thin film oxides are difficult because the thin films typically have 3–4 orders in magnitude less surface area probed by the infrared beam. Often the powders are used as model surfaces for predicting the reactions that occur on the corresponding thin film.

In the case of m-WO_3, collecting infrared data on surface reactions is difficult because, to the best of our knowledge, nano-sized m-WO_3 powders are not commercially available. Commercial WO_3 powders are larger than 1 μm in diameter but are poor materials for infrared studies because they have a low surface area and strongly scatter the infrared beam. Given that nano-sized metal oxide particles can be used to fabricate thick film sensors, the ability to produce small particles of WO_3 would provide dual purposes; it would render the necessary surface area for IR studies of reactions of gaseous molecules on the surface and at the same time, provide material opportunities for the use of nano-sized powders in thick film sensors.

A sol–gel synthesis is the most widely used method to prepare m-WO_3 films.[19,20] A sol can be easily obtained by exchanging a Na_2WO_4 solution through a strongly acidic cation-exchange resin.[21,22] The H_2WO_4 exiting the column is dripped into a reservoir containing water and condenses to form a hydrated tungsten oxide gel. Depending on the reaction conditions, the gel collapses into particles that precipitate from solution. These hydrated tungsten oxide particles convert to micron sized monoclinic WO_3 particles by calcination at 500 °C.

The approaches we use to accomplish a reduction in particle size involve modifying the conditions for the condensation of the H_2WO_4 to form particulate sols. In one synthetic approach, the H_2WO_4 exiting from the ion-exchange column is added to a solution containing oxalic and/or acetic acid. Chelating ligands such as oxalate,[21,23] acetylacetone,[24] and 2,4-pentanedione[25] have been used to generate stable WO_3 sol–gel films. The rate of condensation occurring between two WOH groups is reduced as the number of non-condensable chelating agents attached to the central W atom increases. The slower condensation or cure produces less stress between a sol–gel film and the substrate and this minimizes the cracking that occurs when the film is annealed at elevated temperatures. Sun *et al.*[23,26] have recently reported that the use of oxalate chelating agents also leads to the formation of nano-crystalline WO_3 thin films. While this suggests that nano-particles of m-WO_3 could also be fabricated using a chelating agent, we are unaware of any literature devoted to this particular subject. It is expected that the coordination of the tungstic acid with the oxalate will slow the condensation reaction and inhibit the

DOI: 10.1039/b107993j

growth of larger hydrated tungsten oxide particles. It is also likely that the presence of coordinated ligands will inhibit sintering during the calcination step.

In a second approach, the H_2WO_4 exiting from the ion-exchange column is dripped into a water-in-oil (w/o) emulsion. While this represents a new approach for the fabrication of nano-sized WO_3 particles, the use of emulsions (w/o) using ionic or non-ionic surfactants has been widely used to prepare monodispersed nano-particulate metallic oxides. Copper oxide,[27] silica,[28,29] Fe_2O_3 and TiO_2,[30] as well as nano-structured mixed metal oxides were prepared using emulsion based methods.[31]

A w/o emulsion is composed of continuous phase containing solvent, micro-water-droplets, micelles and free surfactant (see Scheme 1). The conditions leading to droplet-stabilized emulsions for polymerization reactions depend on parameters such as the type and concentration of surfactant, the surfactant : water : organic solvent ratio, the rate of stirring and temperature.[32] In our case, we are limited to non-ionic surfactant systems as traditional cationic or anionic surfactants are salts. These salts have counter-ions such as Na^+ or Cl^- and their presence would lead to mixed tungstates.

The size of the droplet depends on several factors such as molar concentration ratios (water : surfactant : oil),[33–39] nature and length of the alkyl chain of the oil,[33–36] type of surfactant[35,36] and cosurfactant,[38,39] temperature,[33,37] stirring rate and the nature and concentration of the electrolyte solubilized in the water droplets.[33] The main factor influencing the micelle size and droplet size is the molar ratio of water to surfactant. When the concentration of the surfactant in the solvent is higher than the cmc (critical micelle concentration), stable emulsions are formed with micelles containing 50–100 surfactant molecules with a size of 4–6 nm.[40] Micron-sized water droplets are also formed in the emulsion, the size of these droplets is determined by the molar ratio of water : surfactant and is influenced by the stirring rate. In general, the more vigorous the stirring, the smaller the droplets.

The polymerization of the H_2WO_4 occurs in the aqueous phase inside the surfactant stabilized droplets. The surfactant stabilized water droplet behaves as a micro-reactor in which the condensation and hence growth and size of the particle is dependent on the amount of tungstic acid inside each droplet and is ultimately limited by the droplet size. The size of the droplet is in the submicron to micron range and at this size provides a potential means for substantially increasing the surface area of m-WO_3 particles. Furthermore, there is potentially less loss of surface area during the calcination step as individual particles would be encapsulated by surfactant and this should sterically restrict the amount of interparticle sintering.

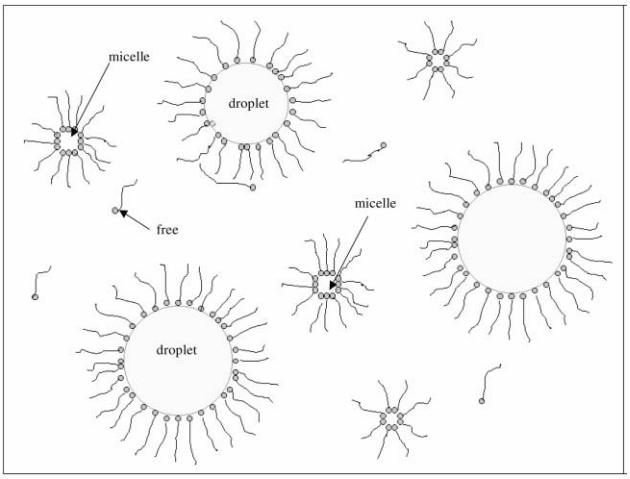

Scheme 1

The synthesized powders derived from the three systems (water only, chelating agents, emulsion) are characterized using scanning electron microscopy (SEM), BET (N_2) surface area, X-ray diffraction (XRD), Raman, and FTIR spectroscopy. Furthermore, we demonstrate the potential use of these nano-sized powders for IR spectroscopic surface studies. Specifically, we compare the infrared data obtained for the adsorption of dimethyl methyl phosphonate (DMMP), a model compound for nerve agents on the synthesized and commercial m-WO_3 powders.

Experimental

Materials

Oxalic acid dihydrate, tungsten(VI) oxide powder 1–5 microns, DMMP, Dowex® 50WX2-200 ion-exchange resin as well as the nonionic surfactants, sorbitan monostearate (Span 60) and sorbitan monooleate (Span 80) were purchased from Aldrich Chemical Company. Glacial acetic acid was purchased from Fisher Scientific Company and toluene was purchased from Alfa Aesar. All chemicals were purchased at their highest commercially available purity and used as received without further purification. Deionized and distilled water (denoted as dd-H_2O, 18 MΩ) was obtained from a Millipore purification system.

Ion-exchange column

Particular care was used to avoid trace sodium ions in generating H_2WO_4 during the condensation step as this would lead to mixed products of WO_3 and sodium tungstate.[41] Furthermore, the presence of counter anions affect the polymerization process and the final solid product.[42–44] All glassware was rinsed thoroughly with dd-H_2O several times before use. Approximately 35 g of the ion-exchange resin was loosely packed in a standard 50 mL burette (1 cm internal diameter). Water was added to the column until the eluant pH was at a stable value of about 5–6. Unless specified otherwise, a 0.12 M $Na_2WO_4 \cdot 2H_2O$ solution was added to a hydrogen ion-exchange column and 20 mL of the eluant was collected at a rate of 0.5 mL min^{-1}. Experience has shown that using higher concentrations of Na_2WO_4 or less resin in the column leads to mixtures of WO_3 and sodium tungstate whereas, using more resin clogged the column with polymerized WO_3 sol.

Sol synthesis

The H_2WO_4 exiting the ion-exchange column was dripped into a beaker containing either water, a solution containing oxalate/acetate ions or a w/o emulsion. In the water only processes, the reaction parameters that were varied included the volume of water (200 mL–4 L), pH (1.5–9) and stirring times from 24 h to 72 h at temperatures from ambient to 45 °C. The natural pH of the tungstic acid in water was about 1.5 and was adjusted by adding NH_4OH. The excess water was then decanted from the precipitated hydrated tungsten oxide ($WO_3 \cdot 2H_2O$) and the powder was dried at 150 °C to remove the remaining water. The $WO_3 \cdot 2H_2O$ was converted to m-WO_3 by calcination at 500 °C. The temperature was ramped from 25 to 500 °C in increments of 5 °C min^{-1} and held constant at 500 °C for 2 h followed by cooling to room temperature.

When using chelating agents, the sol was dripped into aqueous solutions containing various concentrations of acetic acid, oxalic acid, and both oxalic–acetic acid mixtures. Additional variables included pH and reaction time. As with the water only synthesis, excess water was evaporated at 150 °C and the powders were heated to 500 °C at increments of 5 °C min^{-1} and held constant at 500 °C for 2 h followed by cooling to room temperature. This calcination step eliminated the coordinated oxalate/acetate and generated m-WO_3.

For emulsion based methods, we are limited to non-ionic surfactant systems and the choice of surfactants is based upon their HLB (hydrophilic–lipophilic balance) value. This should be between 3 and 6 for a w/o emulsion. The HLB values have been tabulated for a number of surfactants and for our research we have selected two non-ionic surfactants, Span 60 and Span 80 dissolved in toluene. This system has been used to generate w/o emulsions.[45] The structures of Span 60 and Span 80 are shown below.

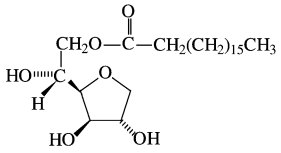

Span-60

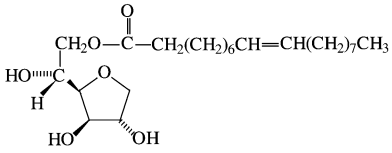

Span-80

The surfactant: toluene ratio was first prepared by dissolving a known quantity of Span 60 or Span 80 in 200 mL of toluene. The water : surfactant : toluene ratio was determined by adding the tungstic acid exiting the ion-exchange column directly into a vessel containing the surfactant–toluene at a rate of about 0.5 mL min^{-1}. During the addition of the tungstic acid, the surfactant–toluene was vigorously stirred at 1000–1600 rpm. In some experiments the concentration of tungstic acid added to the surfactant–toluene was varied. The concentration of tungstic acid was adjusted by changing the concentration of the $Na_2WO_4 \cdot 2H_2O$ solution added to the top of the ion-exchange column. In all cases, the addition of the aqueous solution caused an immediate clouding of the stirred surfactant–toluene solution indicative of the formation of an emulsion.

The high-speed stirring continued for 5 min after the addition of tungstic acid followed by a gentler magnetic stirring (300 rpm) for the following 72 h. During the entire stirring, a single cloudy phase suspension was observed. The emulsion was then left to sit in a sealed container for an additional 48 h to ensure complete reaction.

Removal of the water and toluene was accomplished by evaporation to dryness at room temperature. This typically required 24 h. During the evaporation, the water : surfactant : toluene ratio is constantly changing and a different behavior was observed for the Span 60 and Span 80 based systems. In the Span 60 emulsion, a clear upper phase (toluene) appeared and the lower phase remained cloudy. The lower cloudy phase remained until removal of all solvent. In the case of Span 80 based systems, as the evaporation proceeded, three phases appeared; an upper toluene phase, a middle cloudy slice, and a lower aqueous phase region.

In order to remove the surfactant, and to convert the hydrated tungsten oxide to m-WO_3, the powder was calcined at 500 °C. Samples were transferred to a furnace, heated to 500 °C at a rate of 5 °C min^{-1} and kept at that temperature for 6 h, and then cooled to room temperature at a rate of 20 °C min^{-1}. The oxidation of the surfactant at 500 °C was more difficult to accomplish than observed for the removal of the chelating agents. In some samples, particularly high surfactant loading, removal of the surfactant required prolonged heating (12 h) at higher temperature (550 °C).

Characterization

The calcined powders were first analyzed by Raman and infrared spectroscopy. Raman was used because of the ease in identifying characteristic bands for sodium tungstates, hydrated tungsten oxide and WO_3.[22,25,46–49] For all samples, characteristic sodium tungstate bands at 940–960 cm^{-1} were not detected.[22] Fig. 1a,b shows the Raman spectra of the commercial powder and a typical sample prepared either using the chelating agents or emulsion method. For comparison, a spectrum of the hydrated tungsten oxide is shown in Fig. 1c. The similarity in the spectra of both samples (Fig. 1a and 1b) show that little, if any, hydrated tungsten oxide remains upon calcination. Major Raman bands at 809 and 718 cm^{-1} (W–O stretching modes) and 271 and 131 cm^{-1} (W–O bending modes) as shown in Figs. 1a and b and are characteristic of monoclinic WO_3. Miyakawa *et al.*[22] have shown that the Raman bands at 809 and 718 cm^{-1} were observed for m-WO_3 and do not change as a function of temperature indicating the formation of a highly stable monoclinic crystalline WO_3 at temperatures up to 500 °C. On the other hand, the Raman spectrum of the hydrated WO_3 powder shows that the W–O stretching modes became broad and the Raman mode at 718 cm^{-1} is shifted to 702 cm^{-1} (see Fig. 1c). Both the shift and the shape of the 718 cm^{-1} peak are mainly due to the change in crystal symmetry as well as to lattice distortion.[50] Raman spectra were collected using a Renishaw Raman Imaging Microscope System 1000. The system is equipped with a diode laser having $\lambda_{ex} = 785$ nm. Signal detection is achieved through the used of a sensitive charge coupled device (CCD) array detector.

Infrared spectroscopy was used to ensure removal of residual surfactant or chelating agents (absence of C–H modes) and as a quick assessment of particle size and surface area. In brief, a smaller particle size exhibits less scattering of the infrared beam and higher surface area particles are accompanied by more intense surface WOH and adsorbed water modes. Diffuse reflectance infrared Fourier transform (DRIFT) spectra were recorded on the neat powder and the ratio of intensity of the adsorbed water mode at 1620 cm^{-1} to a bulk mode at 2063 cm^{-1} was used to quickly assess relative surface areas of the WO_3 particles.

In DMMP adsorption experiments, transmission spectra

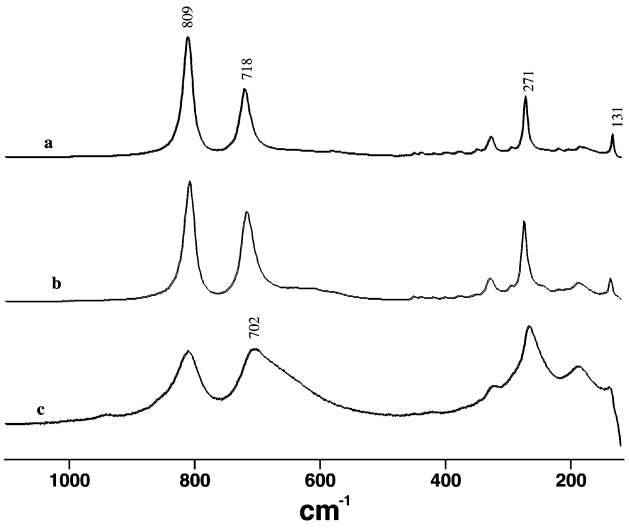

Fig. 1 Raman spectra for: (a) Aldrich m-WO_3 powders; (b) m-WO_3 powders prepared using a non-ionic surfactant and treated at 500 °C for 6 h; and (c) hydrated WO_3 powders.

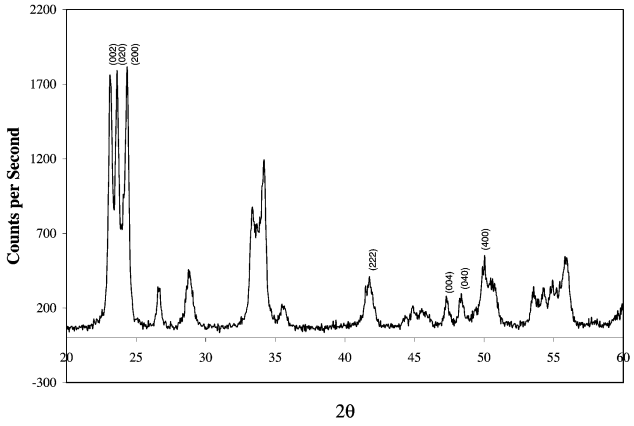

Fig. 2 XRD spectrum of WO_3 powders prepared with oxalic and acetic acids annealed at 500 °C.

were recorded using a thin film technique.[51] Standard vacuum line techniques were used to introduce the DMMP gas. Difference spectra are plotted where the reference spectrum is recorded using the thin film m-WO_3 evacuated at room temperature. Therefore, positive bands are due to bonds that formed on the surface and negative bands represent bond removal from the surface due to DMMP adsorption. The results obtained on the synthesized nano-sized particles were compared to the results obtained with the commercial m-WO_3 powder. FTIR spectra were recorded on a Bomem MB-Series with a liquid N_2 cooled MCT detector. Typically 200 scans were co-added at a resolution of 4 cm^{-1}.

Although we used DRIFT spectra as a quick gauge of relative surface area, all samples were eventually measured for BET (N_2) surface area. BET (N_2) data were recorded on a Gemini 2360 surface area analyzer Micromeritics instrument.

Representative samples were analyzed by powder XRD and particle size/shape by SEM. XRD measurements were performed using a X2 Advanced Diffraction System equipped with a copper anode and a single crystal lithium doped silicon Peltier detector, which has a 100% energy absorption from 2–20 keV with a beryllium window thickness of 0.005 in. Fig. 2 shows the XRD pattern for the calcined WO_3 powder that has a surface area of 22 m^2 g^{-1} and is identical to the pattern expected for monoclinic WO_3. All samples calcined at 500 °C gave the same XRD patterns. SEM micrographs were taken on an AMRay 1000. This instrument has a resolution of 7 nm, a magnification range of 20–100 000×, and an accelerating voltage range of 1–30 kV. The powders were mounted on an eucentric goniometer stage, which enabled both tilt and rotation about the viewing axis.

Results and discussion

A search for a commercial source of high surface area m-WO_3 particles met with little success. The best commercial particles that we measured had a surface area of 1.7 m^2 g^{-1} and these particles scattered the infrared beam and had too low a surface area to be suitable for surface infrared transmission studies. From this work with commercial WO_3 powders, we estimated that a particle size reduction of at least a factor of 10 (*i.e.*, about 20 m^2 g^{-1}) is desired for our infrared studies. Given this requirement, our attempt at producing smaller m-WO_3 particles centered on methods of altering the condensation conditions. The results presented in this paper are a summary of the trends obtained for approximately 50 samples prepared in water only, 50 samples with chelating agents and another 25 with emulsion based synthesis. Each sample represented a specific set of reaction conditions for carrying out the condensation of the tungstic acid. Many samples were repeated 2–3 times to test reproducibility and to investigate various calcination schemes. In examining the data *in toto*, there are clear divisions in ranges of surface areas obtained with the three methods. A summary of these findings is listed in Tables 1 and 2. Generally, the surface areas of the samples prepared in water were 3–5 m^2 g^{-1}, chelating agents gave 16–22 m^2 g^{-1} and for emulsion based samples they were in the range of 40–45 m^2 g^{-1}.

Water only synthesis

This is the simplest synthetic approach and the results obtained would serve as a benchmark for our work using chelating agents or emulsions. Samples were prepared by varying dilution, (the H_2WO_4 solution from the ion-exchange column was dripped into various quantities of water giving final H_2WO_4 concentrations ranging from 2.4×10^{-2} to 2.4×10^{-4} M, resident stirring times (24–102 h), temperature (ambient to 45 °C), and pH (1.5–7). The precipitated hydrated tungsten oxide particles were dried and calcined at 500 °C for 2 h. We found that the above reaction conditions have little effect on the final surface area of the particles. The BET (N_2) analysis shows that the surface area obtained by this method was in the range of 3–5 m^2 g^{-1}. While this is below our desired value of 20 m^2 g^{-1}, it was an improvement over the best commercial powders (1.8 m^2 g^{-1}).

The post-processing curing of the hydrated tungsten oxide at 500 °C is needed to convert the hydrated tungsten oxide to a

Table 2 A summary of the experimental details used to prepare m-WO_3 powders *via* the emulsion method. All samples were stirred for 72 h in 200 ml of toluene

Surfactant	Eluant/mol	Amount of the surfactant added/g	Surface area/m^2 g^{-1}
Span 60	2.4×10^{-2}	5	20.7
		10	45.0
		20	42.7
	6.0×10^{-3}	10	30.0
	1.2×10^{-2}	10	27.4
Span 80	1.2×10^{-3}	5	9.7
		10	3.8
		20	13.0

Table 1 A summary of the experimental methods that led to the synthesis of m-WO_3 powders with the highest surface area using each method

Strategy[a]	Eluant added/mL	Ligand added/mol	Water/mL	pH	Gel time/h	Surface area/m^2 g^{-1}
Sol–gel in water	20	—	400	7	72	5.0
Freeze-fracture, liquid N_2	20	—	400	1.23	48	7.5
AA ligand	20	0.7	1000	2.28	72	3.8
AA ligand	20	0.7	1000	7	72	9.3
OA ligand	20	0.22	1000	1.2	24	17.5
OA ligand	20	0.22	1000	7	24	19.0
AA and OA mixture	20	1 : 1	1000	1.19	72	17.4
AA and OA mixture	20	1 : 1	1000	7	72	22.0

[a]AA, acetic acid; OA, oxalic acid.

monoclinic WO_3 and this step plays a role in dictating particle surface area. In a sol–gel synthesis, the higher the calcination temperature, the greater the sintering and thus the higher the reduction in particle surface area. In our case, we obtain a reduction in surface area (factor of 2.5) for water only samples and those prepared using chelating or emulsion based methods by simply raising the calcination temperature from 500 to 550 °C. However, at temperatures below 500 °C the conversion to m-WO_3 is not complete and with time, the material reverts back to an amorphous hydrated tungsten oxide. Therefore all calcination was done at 500 °C.

The temperature ramp also affects particle size. A slower ramp is generally preferred, as a fast temperature rise often leads to a collapse of the network structure and a reduction in surface area. We observed a progressively higher surface area with slower temperature ramps in going from 20 °C min^{-1} to 5 °C min^{-1} and little change with slower ramps below 5 °C min^{-1}. The typical change in slowing the ramp from 20 °C min^{-1} to 5 °C min^{-1} was an increase of 50% in surface area. Given this result, the general heating protocol was to raise the temperature to 500 °C at a 5 °C min^{-1} ramp.

Some success in increasing the surface area for water based samples was obtained by the addition of a post-processing step. A 0.12 M tungstic acid solution from the ion-exchange column was collected in a beaker. Aliquots were extracted at different gel incubation times, placed in a test-tube and cooled rapidly by immersing in liquid N_2 for 10 min. It required about 1 min to immerse a tube containing the sample into the liquid nitrogen. After 10 min, the tube was removed and allowed to warm to ambient conditions. The gel was destroyed by the rapid cooling process and yellow particles appeared at the bottom of the test-tube. A rapid reduction in temperature leads to a shattering of the gel structure and smaller particulate fragments. After calcination at 500 °C, the liquid N_2 process produced particles that had surface areas of between 6 and 7 $m^2\ g^{-1}$ as compared to 4–5 $m^2\ g^{-1}$ obtained without this step.

Acetate/oxalate chelating agents

It is a common practice to use chelating agents to slow the condensation step in the sol–gel formation in order to form stable and robust metal oxide films. The chelating agents bind to the $H_2WO_4{\cdot}2H_2O$ [or $W(OH)_6$] and this inhibits the condensation and growth of individual particles. The number of bound chelates per W atom is established by several competing equilibrium reactions and therefore depends on several factors such as the type of chelating ligand, the ligand to $H_2WO_4{\cdot}2H_2O$ concentration ratio and pH. Over 50 samples were synthesized by varying the above three factors and the following trends were observed. For both oxalic and acetic acid, the surface area increases with an increase in acid: H_2WO_4 concentration ratio to a plateau value. Typically this value was 0.2 M for oxalic acid and 0.07 M for acetic acid and as a result, all synthesis was performed at a concentration ratio that was a minimum factor of two above this plateau value.

The surface area obtained is highly sensitive to pH for acetic acid and relatively insensitive for oxalic acid based solutions. Addition of the H_2WO_4 to a solution containing acetic acid results in m-WO_3 particles with a low surface area of 3.8 $m^2\ g^{-1}$. This is not surprising because the natural pH of the H_2WO_4 is 1–2 and given that the pK_a of acetic acid is 4.76 there would be few acetate ligands available to bind to the tungsten acid. However, when the pH of the acetic acid solution is adjusted to 7 using NH_4OH, we obtain particles with surface areas increasing to about 9.3 $m^2\ g^{-1}$.

While acetic acid based preparative methods produced slightly higher surface area particles compared to water only synthesis, a marked increase was observed in oxalic acid based solutions. Unlike the predominately monodentate acetate ligand [eqn. (1)], the oxalate is a bidentate ligand [eqn. (2)] and is more strongly bound to the tungstate.

$$W(OH)_6 + H_3CCO_2H \rightleftharpoons W(OAc)_6 + H_2O \qquad (1)$$

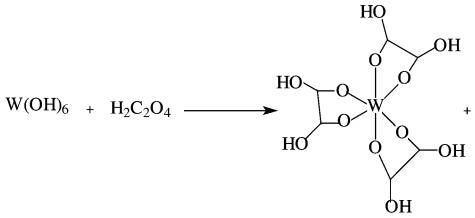

(2)

A nano-sized WO_3 powder with a surface area of 19 $m^2\ g^{-1}$ (BET N_2) was obtained using oxalic acid based solutions at a pH of 7 and no significant change in the particle size was observed by varying the pH from 1 to 7. The oxalate is less sensitive to pH because pK_{a1} for oxalic acid is 1.23 and thus the oxalate anion will be formed at the pH of the sol solution. The surface area of the particles obtained with oxalic acid represent a 10-fold increase in particle size over commercially available material. Varying oxalate concentration (from 0.2–3 M), the pH, and the final volume of the sol–gel solution had little effect and in all cases particles ranging from 16 to 20 $m^2\ g^{-1}$ were obtained.

A further, smaller yet reproducibly higher increase in surface area is obtained when the sol was added to a mixture containing a 1 : 1 molar ratio oxalic to acetic acid. BET analysis showed that these particles had a measured surface area of 22 $m^2\ g^{-1}$. The origin of this slight increase is unclear but is most likely due to a slightly higher coordination number of ligands per W atom occurring with a monodentate–bidentate mixture.

For infrared studies there is a need for both high surface area and small particle size. For example, it is easy to record transmission spectra of a 300 $m^2\ g^{-1}$ fumed silica (nonporous, 10 nm) whereas it is difficult to record the spectrum of a 300 $m^2\ g^{-1}$ silica gel because of scattering of the infrared beam. The scattering obtained with silica gels is due to the larger particle size. The silica gels are typically micron diameter in size and the high surface area arises because these materials are highly porous. In our case, each m-WO_3 sample was measured for a BET surface area and from this value an average particle size was computed. For example, using a hard spherical model, a surface area of 20 $m^2\ g^{-1}$ gives a particle diameter of about 40 nm. However, a BET measurement does not take into account that the surface area could be due to the porosity of the material. Thus, surface area measurements are not sufficient to determine the differences in particle size. Therefore, we periodically recorded SEM pictures of our synthesized WO_3 particles to examine particle size. In all cases, there was good agreement with the calculated particle diameter based on surface area measurements and SEM pictures. Fig. 3 shows the SEM photograph for m-WO_3 powders prepared using oxalate chelating agents (19 $m^2\ g^{-1}$). The SEM results show that the oxalate prepared m-WO_3 samples were found to be nano-sized particulates with primary particle sizes of 30–50 nm, which is consistent with the size computed from surface area data.

W/o emulsion synthesis

In the first experiment the amount of Span 60 in 200 ml of toluene was varied and the volume and concentration of tungstic acid added to the surfactant–toluene was held constant. In principle, the higher the surfactant concentration in toluene, the smaller the droplet size.[32] The measured surface area of the m-WO_3 particles obtained using three surfactant amounts is given in Table 2. There is a notable increase in surface area for the emulsion based synthesis over those obtained using chelating agents. The lowest surface area

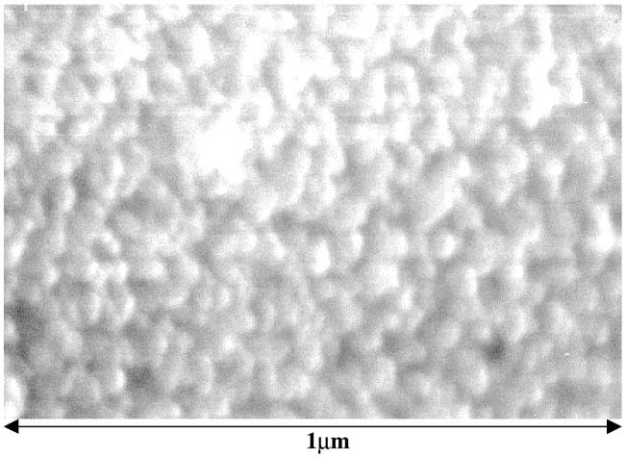

Fig. 3 SEM photographs of the WO_3 samples prepared *via* the sol–gel method using an oxalic acid ligand at pH 7.

obtained using emulsions were on par with the best materials obtained using chelating agents. There was a substantial increase in surface area by doubling the surfactant concentration from 5 g to 10 g and this value leveled with little increase in surface area by adding more surfactant. There is actually a drawback to using too much surfactant, as it was difficult to oxidize and remove the excess surfactant prepared using 20 g of Span 60.

This difficulty in removing the surfactant was experienced in the next experiment where the effect of lowering the amount of tungstic acid in the system was examined. This was accomplished by decreasing the concentration of the tungstic acid. Given that the droplet size is fixed by keeping the surfactant: toluene ratio, stirring rate and volume of elutent constant, a decrease in concentration limits the particle growth because the amount of tungstic acid per droplet is lowered. The surface areas obtained for these samples are given in Table 2 and show that a lowering in concentration of tungstic acid requires a higher calcination temperature to fully remove the surfactant, which, in turn, leads to fusing of the particles and subsequent reduction in surface area.

Examination of the samples by Raman spectroscopy showed that the samples prepared with lower concentrations or lower volumes of tungstic acid contained a significant amount of hydrated tungsten oxide. This was a common feature found for samples that had high surfactant to tungstic acid ratios (*i.e.*, increased surfactant loading or lower tungstic acid amount). In order to convert the samples to m-WO_3 we found that we needed to heat the samples to a higher temperature of 550 °C for a longer time of 12 h. This calcination protocol leads to a reduction in surface area. We find that m-WO_3 samples prepared with water only or chelating agents that are heated under these same conditions showed a decrease in surface area by a factor of 2.5 times over those samples calcined under the standard conditions of 500 °C for 2 h.

The surface area measured for samples prepared using Span 80 are shown in Table 2. In these samples the volumes of toluene and tungstic acid were held constant and the amount of surfactant was varied. All samples produced surface areas much below those obtained with Span 60 or with oxalate chelating agent (see Table 2). We attribute this lower surface area to the three-phase separation leading to an aqueous phase during the initial solvent evaporation stage. One of the principle roles of the surfactant or chelating agent is to prevent aggregation and sintering during the calcination stage. With Span 80, the solvent evaporation leads to the loss of stabilized water droplets and an aqueous phase containing the hydrated tungsten oxide appears. The particles aggregate to larger structures with few surfactant molecules available to sterically prevent sintering upon calcination.

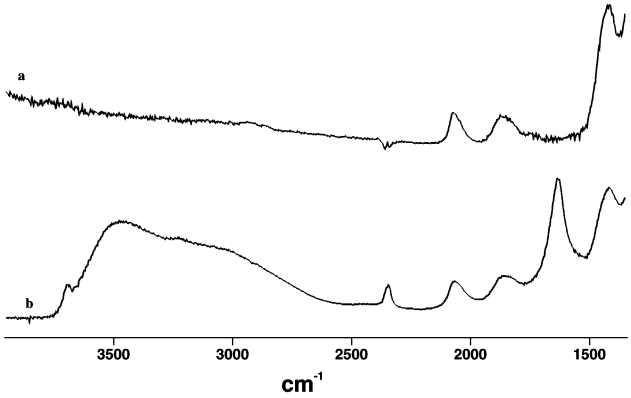

Fig. 4 DRIFT spectra for: (a) Aldrich WO_3 powders and (b) WO_3 samples prepared by dripping the sol into a mixture of acetic and oxalic acids and treated at 500 °C for 6 h.

IR studies

The DRIFT spectra of a medium range area (about 19 m^2 g^{-1}) powder synthesized using oxalate chelating agent and that recorded for a commercially available powder is shown in Fig. 4. The higher surface area enabled detection of bands due to surface OH and adsorbed water in the 3700–3100 cm^{-1} region. Specifically, the broad bands at 3450 and 3692 cm^{-1} are due to various O–H stretching modes and a sharp peak at 1620 cm^{-1} is the H_2O bending mode. In contrast, no bands were observed in the region 3400–3700 cm^{-1}or at 1620 cm^{-1} (see Fig. 4a) in the DRIFT spectrum of the commercial samples. The relative amount of water adsorbed on the surface (and hence the relative surface areas of the powders) can be measured by ratioing the intensities of the 1622 cm^{-1} water bending mode to that of the surface overtone mode at 2063 cm^{-1}. In recording spectra for various samples (not shown), it was found that the relative amount of water adsorbed agreed with the trend in measured BET surface area and followed the order: emulsion > oxalic/acetic acid mixtures > oxalic acid > acetic acid > sol–gel in water only > commercial WO_3 powders.

There is one additional difference between the spectra of the commercial powders and the nano-fabricated samples. The infrared spectrum for the nano-sized WO_3 also shows a sharp band for CO_2 at 2342 cm^{-1} and this band is not present in the commercial samples or those prepared using water only. This band did not reduce or change upon evacuation and elevation of the temperature up to 400 °C and represents trapped CO_2 formed during decomposition of the surfactant or chelating agents during the calcination step.

Adsorption of DMMP

Fig. 5a,b shows the infrared spectra of the adsorbed DMMP on thin films of commercial WO_3 powders and on the prepared nano-sized m-WO_3, respectively. The infrared spectrum of DMMP adsorbed on a nano-sized WO_3 powder exhibits very intense bands (see Fig. 5b) whereas we do not detect any bands due to adsorbed species on the commercial powders (see Fig. 5a). The amount of the adsorbed DMMP on these two WO_3 samples can be estimated from the DRIFT spectra (not shown) using the integrated peak area of the CH_3 mode at 1314 cm^{-1} to that of a band due to a W–O overtone mode. The amount of DMMP adsorbed on the sample (19 m^2 g^{-1}) is about 15 times larger than the amount of DMMP adsorbed on the commercial powder.

With these higher surface area particles it is now possible to use infrared transmission spectroscopy to monitor the reaction of gaseous molecules with the surface. The advantage of transmission using thin films is that the entire infrared region can be accessed. In DRIFT, the region below 1300 cm^{-1} is not

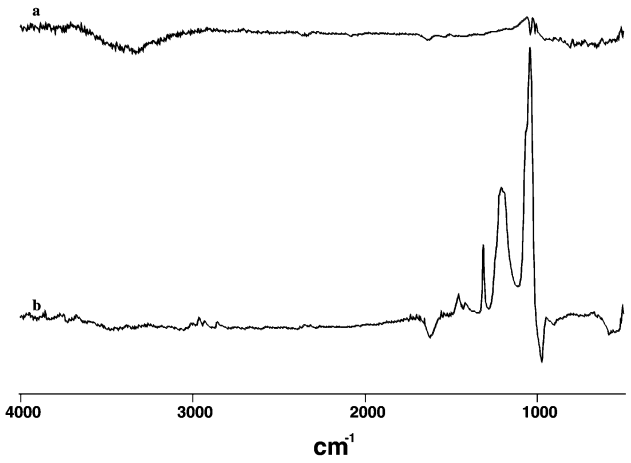

Fig. 5 IR spectra of DMMP adsorbed on: (a) Aldrich WO_3 powders and (b) nano-sized WO_3 powder with a surface area of 45 m^2 g^{-1}.

accessible because of the strong W–O fundamental bulk modes in this region. The importance of the region below 1300 cm^{-1} is shown with the adsorption of DMMP. In this particular example, the O–CH_3 stretching modes of gaseous DMMP at 1042, and 1069 cm^{-1} did not shift upon adsorption. However, the P=O stretching mode shifts from 1276 cm^{-1} in the gas phase to 1209 cm^{-1} upon adsorption. Therefore, adsorption of DMMP on m-WO_3 occurs through the P=O moiety and not through the two methoxy groups.

Conclusion

Synthesis of m-WO_3 in water only, in oxalate/acetate solutions and in w/o emulsions produces particles with surface areas between 2 and 7.5 m^2 g^{-1}, 16 and 22 m^2 g^{-1}, and 40 and 45 m^2 g^{-1}, respectively. A particle of 45 m^2 g^{-1} is equivalent to a 17 nm diameter particle size and this is on par with the smallest particles of metal oxides produced by solution based synthetic methods. For samples prepared using chelating agents, the highest surface areas are prepared using mixed oxalate/acetate solutions. Particles synthesized using only acetic acid had surface areas lower by a factor of 2 than those obtained with oxalic acid. Although emulsion based samples produce the highest surface areas, the use of a high surfactant to tungstic acid ratio should be avoided because this leads to difficulty in removing the surfactant in the calcination of hydrated tungsten oxide to m-WO_3. An important role for both chelating agents and surfactant is that they play a significant role in minimizing the sintering occurring in the calcination step.

It is shown that the high surface area particles are amenable for gas adsorption infrared transmission studies. Specifically, it is shown that DMMP is strongly adsorbed on WO_3 *via* the P=O moiety and no adsorption occurs through the two methoxy groups.

Acknowledgement

We would like to thank the Department of the Navy, Naval Surface Warfare Center, Dohlgren Division, for the financial support, Grant N00178-1-9002.

References

1 X. Wang, N. Miura and N. Yamazoe, *Sens. Actuators, B*, 2000, **66**, 74.
2 C. N. Xu, N. Miura, Y. Ishida, K. Matsuda and N. Yamazoe, *Sens. Actuators, B*, 2000, **65**, 163.
3 E. Comini, G. Sberveglieri, M. Ferroni, V. Guidi and G. Martinelli, *Sens. Actuators, B*, 2000, **68**, 175.
4 D. Lee, K. Nam and D. Lee, *Thin Solid Films*, 2000, **375**, 142.
5 J. L. Solis, S. Saukko, L. Kish, C. G. Granqvist and V. Lantto, *Thin Solid Films*, 2001, **391**, 255.
6 A. K. Akther Hossain, L. F. Cohen, A. Berenov and J. L. Macmanus Driscoll, *Mater. Sci. Eng., B*, 2001, **83**, 79.
7 D. Vincenzi, M. A. Butturi, C. Malagù, V. Guidi, M. C. Carotta, G. Martinelli, V. Guarnieri, S. Brida, B. Margesin, F. Giacomozzi, M. Zen, A. A. Vasiliev and A. V. Pisliakov, *Thin Solid Films*, 2001, **391**, 288.
8 E. Traversa, Y. Sadaoka, M. Carotta and G. Martinelli, *Sens. Actuators, B*, 2000, **65**, 181.
9 D. Vincenzi, M. A. Butturi, V. Guidi, M. C. Carotta, G. Martinelli, V. Guarnieri, S. Brida, B. Margesin, F. Giacomozzi, M. Zen, G. U. Pignatel, A. A. Vasiliev and A. V. Pisliakov, *Sens. Actuators, B*, 2001, **77**, 95.
10 E. Laperdrix, A. Sahibed-dine, G. Costentin, M. Bensitel and J. Lavalley, *Appl. Catal., B*, 2000, **27**, 137.
11 S. Takeda, M. Fukawa, Y. Hayashi and K. Matsumoto, *Thin Solid Films*, 1999, **339**, 220.
12 D. M. Smyth, *Solid State Ionics*, 2000, **129**, 5.
13 M. C. Kung and H. H. Kung, *Catal. Rev. Sci. Eng.*, 1985, **27**, 425.
14 K. D. Dobson and A. J. McQuillan, *Spectrochim. Acta, Part A*, 1999, **55**, 1395.
15 A. Zecchina, D. Scarano, S. Bordiga, G. Ricchiardi, G. Spoto and F. Geobaldo, *Catal. Today*, 1996, **27**, 403.
16 J. Raskó, E. Novák and F. Solymosi, *Catal. Today*, 1996, **27**, 115.
17 C. Morterra and G. Magnacca, *Catal. Today*, 1996, **27**, 497.
18 M. A. Vuurman and I. E. Wachs, *J. Phys. Chem.*, 1992, **96**, 5008.
19 K. Lee, *Thin Solid Films*, 1997, **302**, 84.
20 A. Chemseddine, R. Morineau and J. Livage, *Solid State Ionics*, 1983, **9/10**, 357.
21 M. Deepa, N. Sharma, S. Varshney, S. Varma and S. A. Agnihotry, *J. Mater. Sci.*, 2000, **35**, 5313.
22 K. Nonaka, A. Takase and K. Miyakawa, *J. Mater. Sci. Lett.*, 1993, **12**, 274.
23 M. Sun, N. Xu, Y. W. Cao, J. N. Yao and E. G. Wang, *J. Mater. Sci. Lett.*, 2000, **19**, 1407.
24 J. Livage, M. Henry and C. Sanchez, *Prog. Solid State Chem.*, 1988, **18**, 259.
25 T. Nishide and F. Mizukami, *Thin Solid Films*, 1995, **259**, 212.
26 N. Xu, M. Sun, Y. W. Cao, J. N. Yao and E. G. Wang, *Appl. Surf. Sci.*, 2000, **157**, 81.
27 M. Pileni and I. Lisiecki, *Colloids Surf., A*, 1993, **80**, 63.
28 H. Ono and K. Takahashi, *J. Chem. Eng. Jpn.*, 1998, **31**, 808.
29 F. Arriagada and K. Osseo, *J. Colloid Interface Sci.*, 1995, **170**, 8.
30 W. Sager, H. Eicke and W. Sun, *Colloids Surf.*, 1993, **79**, 199.
31 A. Zarur and J. Ying, *Nature*, 2000, **403**, 65.
32 J. Lang, N. Lalem and R. Zana, *Colloids Surf.*, 1992, **68**, 199.
33 J. Lang and A. Jada, *J. Phys. Chem.*, 1988, **92**, 1946.
34 A. Jada, J. Lang and R. Zana, *J. Phys. Chem.*, 1989, **93**, 10.
35 A. Jada, J. Lang and R. Zana, *J. Phys. Chem.*, 1990, **94**, 381.
36 R. Zana and J. Lang, *J. Phys. Chem.*, 1991, **95**, 3364.
37 J. Lang, G. Mascolo, R. Zana and P. Luisi, *J. Phys. Chem.*, 1990, **94**, 3069.
38 J. Lang, N. Laiem and R. Zana, *J. Phys. Chem.*, 1992, **96**, 4667.
39 J. Lang, N. Lalem and R. Zana, *J. Phys. Chem.*, 1991, **95**, 9533.
40 V. Pillai, P. Kumar, M. Multani and D. Shah, *Colloids Surf., A*, 1993, **80**, 69.
41 T. Namba, Y. Nishiyama and I. Yasui, *J. Mater. Res.*, 1991, **6**, 1324.
42 S. Music, A. Vertes, G. W. Simmons and I. Czako-Nagy, *J. Colloid Interface Sci.*, 1982, **85**, 256.
43 M. Gotic, S. Popovic, N. Ljubesic and S. Music, *J. Mater. Sci.*, 1994, **29**, 2474.
44 T. Kinugasa, K. Watanabe and H. Takeuchi, *J. Chem. Eng. Jpn.*, 1992, **25**, 128.
45 S. H. Lee, H. M. Cheong, J.-G. Ahang, A. Mascarenhas, D. K. Benson and S. K. Deb, *Appl. Phys. Lett.*, 1999, **74**, 242.
46 E. W. Forsythe, V. E. Choong, T. Q. Le and Y. Gao, *J. Vac. Sci. Technol., A*, 1999, **17**, 3429.
47 M. Gotic, M. Ivanda, S. Popovic and S. Music, *Mater. Sci. Eng., B*, 2000, **77**, 193.
48 E. Salje, *Acta Crystallogr., Sect A*, 1975, **31**, 360.
49 M. F. Daniel, B. Desbat, J. C. Lassegues, B. Gerand and M. Figlarz, *J. Solid State Chem.*, 1987, **67**, 235.
50 Y. Shigesato, A. Murayama, T. Kamimori and K. Matsuhiro, *Appl. Surf. Sci.*, 1988, **33/34**, 804.
51 C. P. Tripp and M. L. Hair, *Langmuir*, 1991, **7**, 923.